Published in Image Analysis, Sediments and Paleoenvironments, 7, 273-293, 2005
which should be used for any reference to this work

MULTIRESOLUTION ANALYSIS OF SHELL GROWTH INCREMENTS TO DETECT VARIATIONS IN NATURAL CYCLES

ERIC P. VERRECCHIA (eric.verrecchia@unine.ch)

Institut de Géologie
Université de Neuchâtel
Rue Emile Argand 11
2007 Neuchâtel
Switzerland

Keywords: Wavelet transform, Spectral analysis, Fourier analysis, Power spectrum, Shell growth, Freshwater clams, Environmental record

Introduction

In the last ten years, wavelet transform has become a standard method of spectral analysis for digital signals and images. Its ability to cope with both spatial and frequency localizations and its low cost in terms of computational complexity are the main reasons for its success. This paper provides an introduction to multiresolution analysis, which is closely related to discrete wavelet transform. Multiresolution is also called multiscalar analysis, because of its ability to extract information at various scales. Wavelet transform has been compared to a mathematical microscope (Burke Hubbard 1995). An application of multiresolution analysis is taken from environmental sciences, using shell growth increments to illustrate variations in environmental conditions. After a short overview of the reasons that have led to the concept of wavelet analysis, special emphasis will be put on the use of wavelet and scaling bases. The reconstruction technique, which allows a particularly simple and natural presentation of the results, will be also discussed.

Spectral analysis

The principle of spectral analysis

Spectral analysis of a given signal (variations of an element's concentration through time, variations of bed thickness, etc.) is mainly based on the decomposition and the projection of the initial raw signal onto a new space, where it is possible to distinguish the various elements (signals or functions) composing the initial data. In other words, spectral analysis is a kind of principal component analysis in which each signal is decomposed into a sum of elementary signals projected onto a new orthogonal space (equivalent of principal components). Each

axis (each principal component) in this space represents a part of the signal variance. Obviously, the initial signal can be reconstructed by summing all its elementary signals (the sum of all principal component variance is equal to the total variance of the initial data set). Each decomposition can be inverted for signal reconstruction: the reconstruction is the operation going from the space of projection back to the initial signal space. However, during reconstruction, the initial signal can also be filtered by using only part of its decomposition, ignoring for example signals bearing low information (low variance). Therefore, the principle of spectral analysis is the following: the raw signal is projected onto another space where it can be decomposed in a new orthonormal basis where each element includes a part of its variance, and then some part of the decomposition elements are selected to reconstruct a filtered signal by an inverse method.

A corollary of this principle is that it can provide information on the elementary signals that contain the most important part of the initial signal information (the most important variance). Therefore, it is possible to identify which signals are the most important components of the raw initial signal. If the initial signal is a function of time, it will be possible to detect the main frequencies composing it. In terms of paleoenvironments, this means that some important natural periodic events, such as tides, sun spots, or Milankovitch cycles, can be detected from natural variables recorded through time (bed thickness, calcium carbonate content, major or trace elements concentrations, etc., see Schwarzacher (1993)). The most conventional method used for spectral analysis is Fourier analysis.

Fourier analysis

Fourier analysis is based on the principle that a composite signal of a period T can be decomposed into a sum of constant and trigonometric functions between 0 and 2π, and respectively of periods T, $\frac{T}{2}$, $\frac{T}{3}$, ..., $\frac{T}{n}$, according to the expression:

$$\begin{aligned} S_n(x) &= A_0 + A_1 \cdot \cos\left(\frac{2\pi}{T}t + \varphi_1\right) + A_2 \cdot \cos\left(\frac{2\pi}{T}2t + \varphi_2\right) \\ &\quad + A_3 \cdot \cos\left(\frac{2\pi}{T}3t + \varphi_3\right) + \cdots + A_n \cdot \cos\left(\frac{2\pi}{T}nt + \varphi_n\right). \end{aligned} \tag{1}$$

The different values of A_n are called the amplitudes of the various n harmonics, which are the n trigonometric elements of the sum. Therefore, the harmonics are elementary sinusoidal functions of periods T, $\frac{T}{2}$, $\frac{T}{3}$, ..., $\frac{T}{n}$ with their associated φ_n, which are the phases at the origin, i.e., the difference between the origin and the starting point of the function on the Oy axis. The Fourier series is characterized by a graph or a bar chart, called a spectrum, on which each harmonic is plotted in function of its associated amplitude. Let us take a simple example to illustrate the relationships between a signal and the spectrum of its Fourier series.

The graph in Figure 1 gives the shapes of a series of sinusoids of increasing frequencies ($1F$, $2F$, $3F$, $5F$, and $7F$). Imagine that we sum all of these functions, but we subtract the fifth one and we double the values of the third one. The composite signal obtained is defined by the following equation:

$$f(x) = \sin(x) + \sin(2x) + 2\sin(3x) - \sin(5x) + \sin(7x). \tag{2}$$

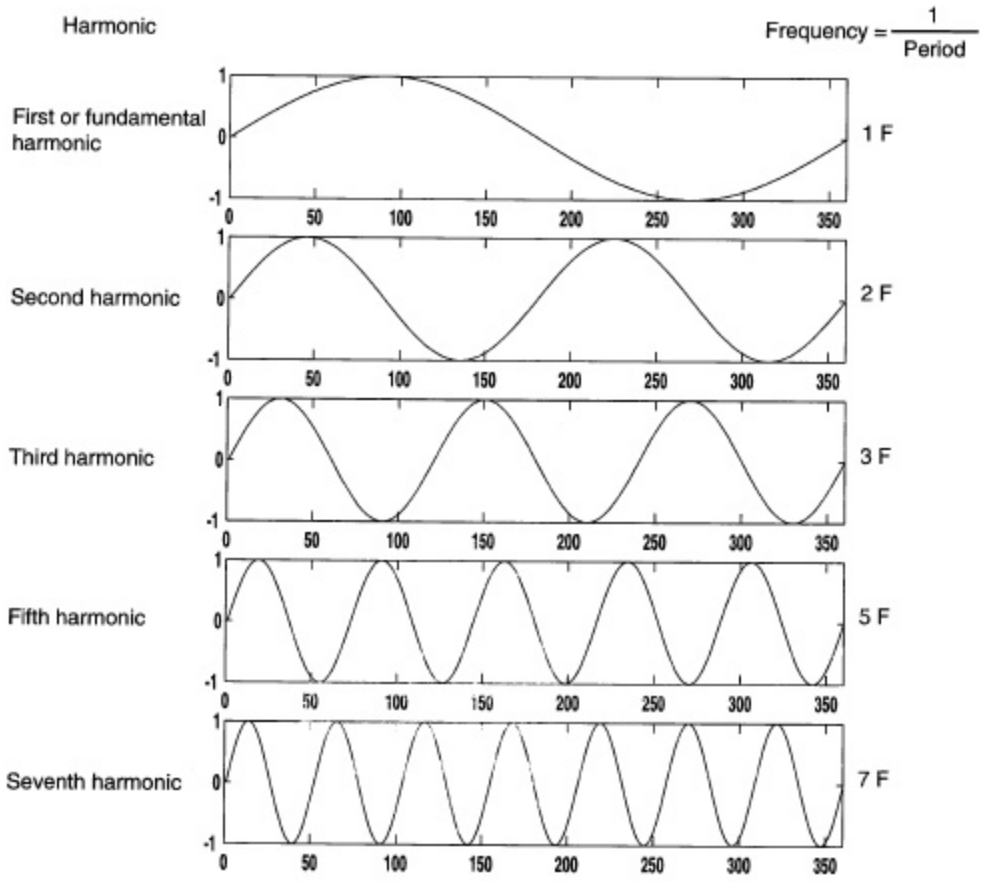

Figure 1. Notation in terms of harmonics and frequencies of elementary signals.

The Fourier spectrum of this composite signal (see Fig. 2) is the picture of the value (the amplitude) of each function (each harmonic) we have summed. Therefore, the spectrum is supposed to give the amplitudes of the various harmonics in ascending order, i.e., harmonics 1 (for the first frequency, called the fundamental harmonic), 2 for the second frequency, and so on. In equation (2), the frequency of the signal is given by the successive values in front of the variable x and the amplitude by the multiplicative coefficient in front of the function. In conclusion, the first, the second, and the seventh harmonics have an amplitude of 1, whereas the fourth and the sixth harmonics, have an amplitude of 0 (they do not appear in the equation, i.e., the sum). The third harmonic has an amplitude of 2 and the fifth harmonic an amplitude of -1. Nevertheless, because $-\sin(5x) = \sin(5x + \pi)$, the amplitude is considered to be 1, but the phase is π. All the other harmonics have a phase equal to 0. The Fourier spectrum of the function given in equation (2) is a bar chart showing only the amplitudes (Fig. 2).

The function given in equation (2) describes a stationary signal, which means that the signal is invariant through translation. In this case, the solution of the Fourier analysis is

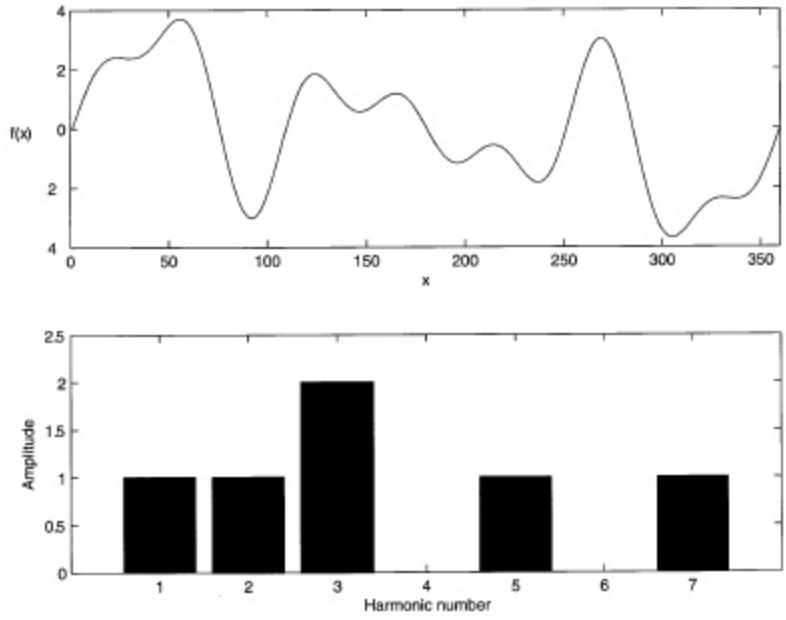

Figure 2. Top: graph of a complex function resulting from equation (2). Bottom: graph of the Fourier series of the top signal showing the amplitude of the seven first harmonics.

trivial. But for non-stationary signals, such as natural images, the solution is not obvious and the interpretation is often fairly complex. The spectrum loses all the local information and therefore makes the interpretation in terms of space (or time) almost impossible (Fig. 3).

To summarize, Fourier analysis, and its operator the Fourier transform, allows space to be changed by projecting the signal into Fourier space where it is represented by the various frequencies composing the original signal. The Fourier transform of a signal is given by:

$$\widehat{f}(\omega) = T^{\text{Fourier}} f(\omega) = \int_{-\infty}^{+\infty} f(t) e^{-i\omega t} dt, \tag{3}$$

where $\widehat{f}(\omega)$ describes the spectral behavior of the function $f(t)$. Nevertheless, during the integral (or summation) calculation, all time and space location information is lost for non-stationary signals. Other methods have to be found to keep local information and frequencies.

Wavelet transform

The advantage of wavelet transform

In the Fourier transform of a signal, the information given is a spectrum in which the main harmonics and their respective amplitudes can be seen. Nevertheless, the local information is lost and the spectrum is an image of the signal as a whole. For example, a bird song can be considered as a succession of various notes. By analyzing this "song signal" using the

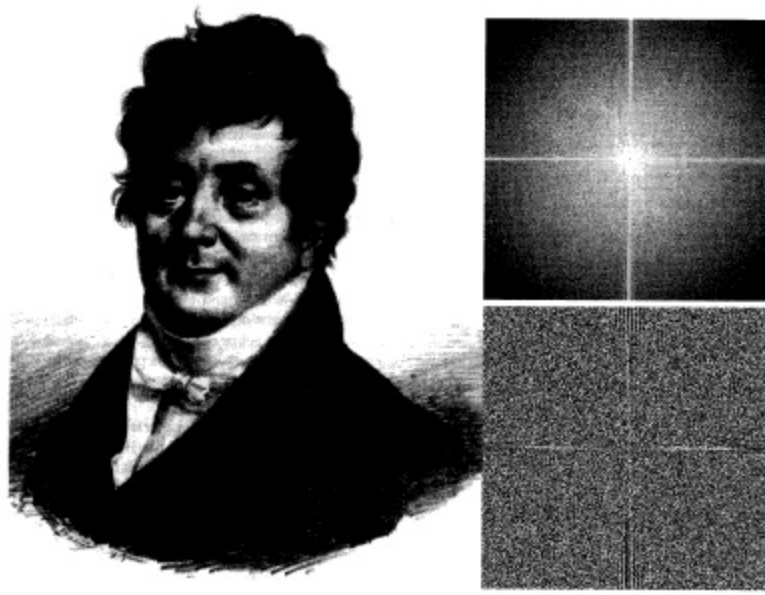

Figure 3. Fourier portrait and its Fourier transform. On the top right: moduli (amplitudes). On the bottom right: phases.

Fourier transform, it is possible to determine if these notes are present in the song and their respective amplitudes. However, Fourier analysis is not capable of determining at what time a particular note appears in the song, i.e., the location information is lost.

This lack of location information in Fourier analysis has been noticed by Gabor (1946). An attempt to keep the spatial location of information characterized by some specific spectral properties led to the concept of the sliding windowed Fourier transform. The associated transform to this operator is called the short time Fourier transform (STFT) or windowed Fourier transform. The function, or moving window $g(s-t)$ where t is the translation parameter, is applied to the signal and the Fourier transform is applied to the signal within the window as the window is moved. The general formula of this transform is (see for example Truchetet (1998) or Addison (2002)):

$$T^{\mathrm{STFT}} f(t,\omega) = \int_{-\infty}^{+\infty} f(s) g(s-t) e^{-i\omega s} ds. \tag{4}$$

This transform is identical to the conventional Fourier transform, but with a multiplication of the exponential member by a window function. The t parameter is a translation parameter allowing the preservation of the time aspect of the signal during the transform. Therefore, the signal is analyzed in a window of a fixed dimension. The tiling in the spatio-frequency domain is the same for all frequencies. Unfortunately, the window is too narrow for low frequencies, but not narrow enough for high frequencies. In conclusion, this analysis is not optimal: it is obvious that a good frequency accuracy at high frequency needs less space (for a given number of periods) than at a lower frequency. To conclude on short time Fourier transform, the result is an analysis taking into account the time domain, but in

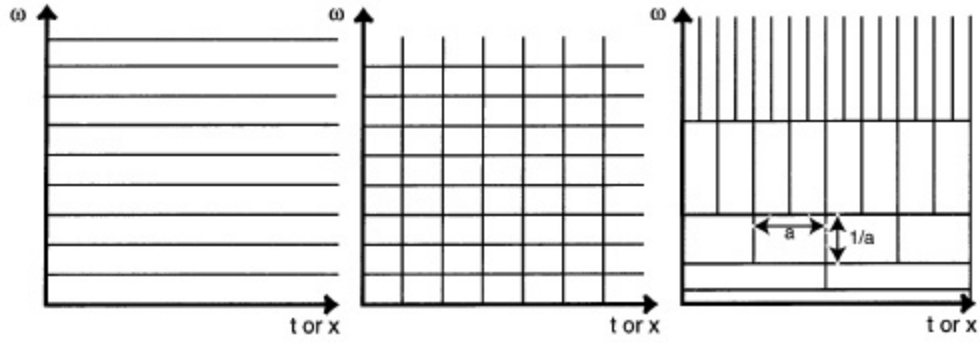

Figure 4. The tiling aspect of the time-frequency domain for the three main transforms. From left to right, Fourier transform, short time Fourier transform, wavelet transform. On the abscissa axis, the variable x or t represents space or time. On the ordinate axis, the variable ω represents the frequencies. Low values of ω are equivalent to low frequencies, and high values of ω to high frequencies. In the wavelet tiling of time-frequency domain, the low frequencies represent the large scales, whereas the high frequencies correspond to the small scales (the scale factor a plays the role of the inverse of the frequency).

which the quality of the frequency analysis is good only for average frequencies (neither low nor high).

The tiling aspect of the time-frequency domain is illustrated in Figure 4. In the conventional Fourier transform, the signal is decomposed into various frequencies, but the graph does not give any information on the location of these frequencies. In the STFT, the regular tiling preserves part of local but fixed information on the frequencies, although it is not accurate for low or high frequencies. On the contrary, this trade off between spatial and spectral resolution is naturally provided by wavelet transform, in which stretching and translation of a unique analyzing function, called the "mother wavelet", is used to scan the whole spatio-frequency domain.

Wavelet transform theory

The continuous wavelet transform has the following expression:

$$T^{\text{wavelet}} f_{a,b}(t) = \frac{1}{\sqrt{a}} \int_{-\infty}^{+\infty} f(t)\psi\left(\frac{t-b}{a}\right)dt, \tag{5}$$

where

$$\psi_{a,b}(t) = \frac{1}{\sqrt{a}}\psi\left(\frac{t-b}{a}\right) \tag{6}$$

is the wavelet function (also called the analyzing wavelet or the mother wavelet), a being the scale factor and b the translation parameter. The a factor takes the role of the inverse of

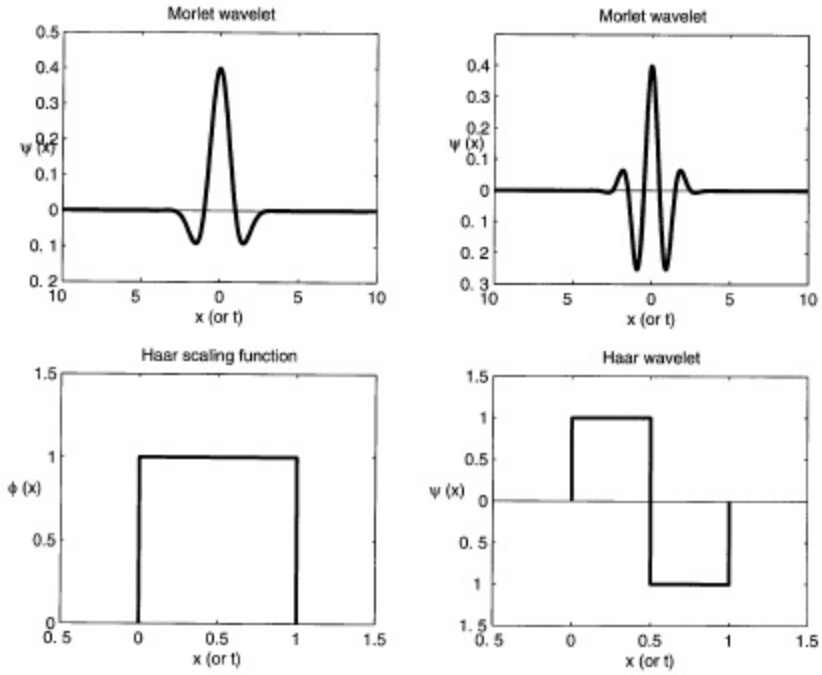

Figure 5. Top: Morlet's mother wavelet with coefficients $\omega_0 = 1/2\pi$ and $\omega_0 = \pi$ in equation (7). Bottom: the Haar scaling function and the Haar wavelet.

the frequency: the smaller a, the less temporally wide the wavelet (the analyzing function), therefore, the higher the central frequency of the spectrum (Truchetet 1998; see Fig. 4).

Historical examples of such mother wavelets are given by Morlet's wavelet:

$$\psi(x) = \frac{1}{\sqrt{2\pi}} e^{-\frac{x^2}{2}} e^{-i\omega_0 x} \tag{7}$$

and the Haar wavelet:

$$\psi(x) = \begin{cases} 1 & 0 \leq t < \frac{1}{2} \\ -1 & \frac{1}{2} \leq t < 1 \\ 0 : & \text{elsewhere.} \end{cases} \tag{8}$$

An example of these mother wavelets is given in Figure 5.

Discrete wavelet transform

If a and b in expression (5) are replaced by the following values $a = a_0^j$ and $b = nb_0a_0^j$ with $n, j \in Z$, then a discrete expression can be introduced, giving the discrete wavelet

transform (DWT) of a continuous signal $f(t)$ (Addison 2002):

$$T^{dwt} f_{j,n}(t) = a_0^{-\frac{j}{2}} \int_{-\infty}^{+\infty} f(t)\psi\left(a_0^{-j}t - nb_0\right)dt. \tag{9}$$

The choice of $a_0 = 2$ and $b_0 = 1$ leads to the dyadic transform. It is certainly the most commonly used wavelet transform and an example of its application will be given later. Nevertheless, other possibilities exist, such as rational values for a_0. In this case, it is common to call j the scale of resolution. A major point is that these transformations can be extended to signal analysis in two or more dimensions. In addition, under given conditions, the wavelet transform has an inverse transform (IWT) like the Fourier transform (IFT). For example, this inverse wavelet transform allows results to be displayed after multiresolution analysis.

Multiresolution analysis

What is multiresolution analysis?

The principle of the multiresolution approach is based on a theory defining linear operators allowing analysis of a signal at various scales. The most well known method is based on Mallat's dyadic algorithm (Mallat 1989a, b, c). A signal $a_n^{(j)}$ including n components at scale j (Fig. 6A) is split into two signals with $\frac{n}{2}$ components, the signal of details and the signal of approximation. Each of these two signals are obtained by applying two filters on $a_n^{(j)}$, $\tilde{h}$ and $\tilde{g}$, their size becoming $\frac{n}{2}$ by suppression of one out of two points. The obtained approximation signal becomes the signal of the scale $i + 1$. Reconstruction of the signal at the scale i from signals at the scale $i + 1$ is obtained by an inverse process: insertion of null samples in order to get signals of size n, application of two filters (conjugates of the former ones), and then summation of the two obtained signals (Fig. 6A).

In other words, the multiresolution approach is a sort of mathematical microscope that can be used to observe a signal from near or far. This zoom-in effect is driven by a scale function that dilates through the various scales. The signal projected onto this function gives a representation of the original signal at a higher scale. This representation (projection coefficients) leads to a backward zooming from the original signal, explaining the term of approximation coefficients used in such operations. To reconstruct the signal from the approximation coefficients, it is necessary to project the original signal onto an orthonormal subspace (to keep all the information). The function generating this second vectorial space is a wavelet. To summarize, the signal is projected onto a scale function, creating an approximation signal, and onto a wavelet to get back all the information lost during the first projection. This second projection includes all the details of the original signal. Finally, the scale function is a sort of low pass filter, whereas the wavelet is a high pass filter. Therefore, details are the high frequencies of the signal.

The multiresolution scheme used in this paper has been proposed by Mallat and Meyer (Mallat 1989a, b, c; Meyer 1990) and is based on an orthonormal projection of the signal to be analyzed onto a series of embedded closed subspaces V_j with $V_j \subset V_{j-1}$. The orthogonal complement of V_j in V_{j-1} is W_j with $V_{j-1} = V_j \oplus W_j$, as explained above and illustrated in Figure 6. An orthogonal wavelet basis exists for these subspaces. This

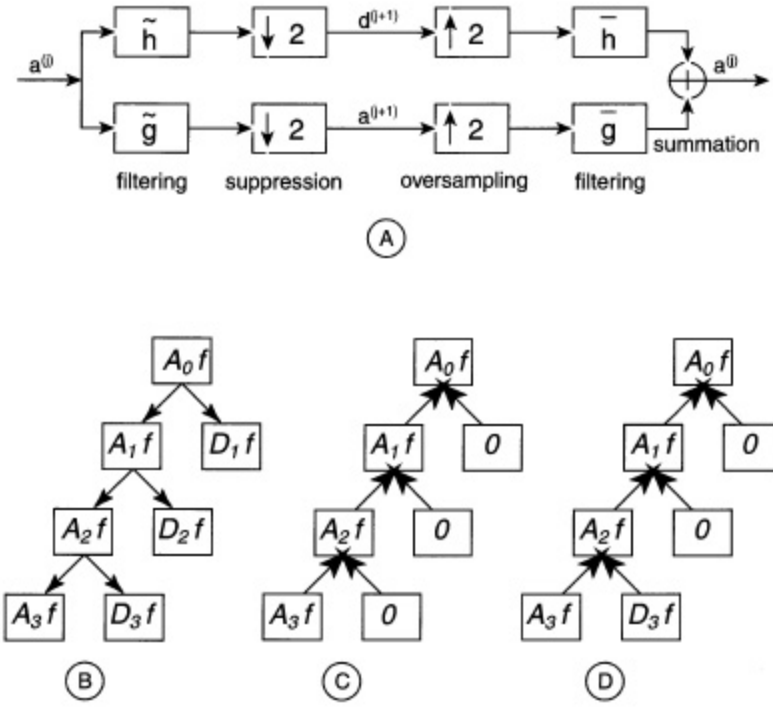

Figure 6. A) Decomposition and reconstruction following Mallat's algorithm. B-C-D) Example of the decomposition and reconstruction of a signal f using 3 scales of resolution. B) Decomposition of signal f in the two different subspaces (detail subspace D and approximation subspace A) at 3 different scales. Each level of approximation is decomposed into two subspaces. C) Reconstruction of a signal by resetting all the detail coefficients ($D_n f = 0$). The signal f at scale 3 is a non-subsampled approximation. D) An example showing a reset of approximation coefficients at scale 3 and detail coefficients at scales <3 in order to reconstruct a non-subsampled view of the details.

multiresolution analysis is dyadic if $f(x) \in V_j \Rightarrow f(2x) \in V_{j-1}$. The a_n^j are called the coefficients of the approximation function (or approximation coefficients) and the d_n^j, the wavelet coefficients (or the detail coefficients) for the scale j. Mallat (1989b) has demonstrated that the projection onto each subspace can be performed by a simple convolution product between the digital signal constituted by the coefficients and a unique digital filter. Taking the scaling function $\varphi(x)$, a wavelet function filter $\psi(x)$ allowing the multiresolution analysis has to be found such that it is orthonormal to $\varphi(x)$ (Daubechies 1988; Viscito and Allebach 1991). By only considering the bi-orthogonality between $\varphi(x)$ and $\psi(x)$, the filters can be built as recursive ones with a low number of coefficients (Delyon 1993). This is exactly the case if a B-spline function is chosen for $\varphi(x)$.

An illustration of multiresolution analysis

In order to illustrate the concept of multiresolution analysis, a natural signal will be decomposed at five different scales, each of them being characterized by its detail and approximation coefficients. The natural signal (s) is built using successive thicknesses of

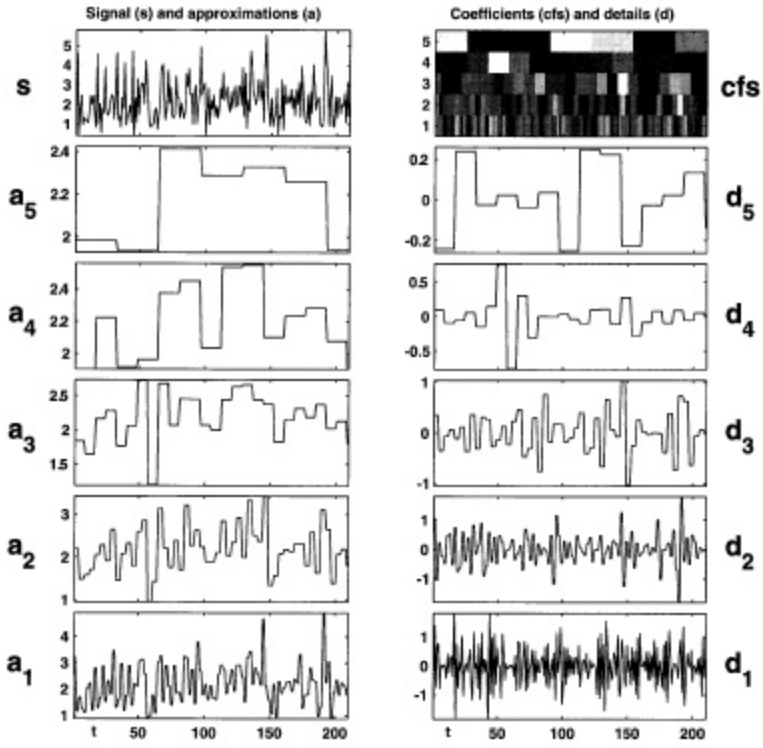

Figure 7. Example of a multiresolution analysis using the Haar wavelet and its associated scaling function (see Fig. 5). In s, the original signal is comprised of the thicknesses of 210 layers of varved sediments from a proglacial lake (Last Glacial Maximum, Jura Mountains, France). From a_5 to a_1, approximation coefficients showing the smoothing effect of the Haar scaling function. In a_1, the smoothing effect is obvious when the graph is compared with the original signal in s. The detail coefficients, from d_5 to d_1, provide the Haar wavelet coefficients calculated for each scale. These coefficients correspond to high frequencies for each scale. Scale-time tiling is given in cfs.

210 layers of varved sediments, deposited in a proglacial lake during the Last Glacial Maximal in the Jura Mountains (France). The thickness in mm is plotted on the y axis and the number of successive laminae is on the x axis (Fig. 7). The mother and scaling wavelets used for the analysis are the Haar wavelets, as shown in Figure 5 and defined in equation (8). The various approximation coefficients (the following a_n with $n \in [1, 2, 3, 4, 5]$) and detail coefficients (the following d_n with $n \in [1, 2, 3, 4, 5]$) have been calculated using the convolution between the Haar scaling wavelet and the Haar mother wavelet, respectively. The results are given in Figure 7. It is obvious that the approximation coefficients, from a_1 to a_5 following the various scales, has a smoothing effect on the initial signal. Compared to the Fourier transform which affects the signal as a whole, this smoothing effect does take into account the distribution of the various peaks, depending on their location, i.e., the local impact (or contribution) of the various frequencies composing the signal. In addition, a signal at a given scale, e.g., 2 is the sum of the detail and approximation coefficients of scale 3. The scale-time tiling given in cfs represents the value of the wavelet coefficient at each scale (from 1 to 5). The tiles are wider at scale 5 because they represent a more dilated function than at scale 1, for example. The lighter the color of the window, the higher the

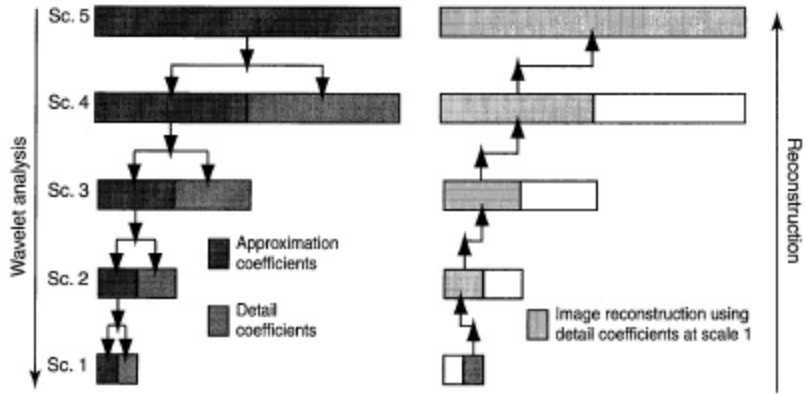

Figure 8. Principle of wavelet and multiscalar analysis. During the wavelet analysis step, a raw image, e.g., at scale 5 (Sc. 5), is filtered into two sub-images constituting the image at scale 4 (Sc. 4), and resulting from the combination of approximation and detail coefficients. This analysis can be performed until scale 1 (Sc. 1), each time by analyzing the detail coefficient image of the former scale level. In the reconstruction step example, only detail coefficients at scale 1 are kept to rebuild the filtered image.

coefficient (in absolute value). Note that all the detail coefficients are centered on the $y = 0$ axis.

A general cascade algorithm

As seen in the paragraph above, the reconstruction of details at scale j is performed by taking the coefficients d_j, computed by the analysis of the signal s, and cancelling all the other coefficients for each of the other scales. These coefficients will constitute the approximation at the zero scale of the projection of the signal s on the subspace W_j (see Fig. 6B, C and D). Technically, the method is divided into two main steps (Fig. 8). First a multiresolution analysis, according to the Mallat algorithm (see Fig. 6A), is processed to compute the approximation and detail coefficients at scale j, giving a_j and d_j. Then, a reconstruction synthesis is made using only the coefficients of approximation and/or detail, corresponding to the explored scale. The result provides a non-subsampled view of the projection at a given scale j. This will be critical to detect variations without losing any information as demonstrated in the following natural example.

Application to growth increment detection

Methodology

The method described above has been used to extract growth increments at various resolutions from Holocene freshwater shells in order to demonstrate that they are able to record environmental fluctuations during their growth. *Anodonta cygnae* L. is a freshwater mussel that has a maximum 18 year lifespan (8–10 years on average). During the biomineralization of their shell, they record environmental variations at various scales, as marine shells do (Rhoads and Pannella 1970). Nevertheless, freshwater environments do not provide

the buffered conditions that the ocean does and it is often difficult to link shell growth increments with periodic and/or regular environmental conditions (Downing et al. 1992). In this particular case, it seems that the best method for environmental signal deconvolution remains wavelet analysis.

The orthonormal basis used in this application is built using cubic B-splines, a symmetric function (Olkkonen 1995). The image is decomposed using multiresolution analysis. At this stage, an approximation of the target projection is reconstructed. For example, the result of the computation for the reconstruction, in which the approximation coefficients have been deleted from the largest scale, is equivalent to the reconstruction of the approximation of $f - A_j f$ (Diou et al. 1999). Since the projection operator is linear:

$$a_0(f - a_j f) = a_0 f - a_0(a_j f) \tag{10}$$

therefore,

$$\begin{aligned} a_0(f - a_j f) &= a_j f + a_1 f + d_2 f + \cdots + d_j f - a_j f, \\ a_0(f - a_j f) &= d_1 f + d_2 f + \cdots + d_j f. \end{aligned}$$

This principle is illustrated in Figure 8, showing the two steps, i.e., coefficient extraction using wavelet transform and reconstruction at the various selected scales using either detail or approximation coefficients. An analysis of detail coefficients at different scales will be performed on the prismatic layer of an *Anodonta cygnae* L. shell. Consequently, the prismatic layer's microtopography has to be recorded as a range image, i.e., a grey level image in which the grey level is related to the relative altitude of each pixel. Detection of the main cycles related to environmental variations will be performed at various scales of resolution, using the relative differences in the microtopography of this prismatic layer. From the raw range image (Fig. 9A), wavelet analysis is used to extract detail coefficients and to reconstruct the filtered image at a given scale (Fig. 9B). A microtopography signal is extracted from this new image in one or two dimensions (Fig. 9C) and a spectral analysis is performed to detect the main cycles (Fig. 9D).

Before any mathematical treatment, the shell topography (Fig. 10A) has to be cleaned in diluted hypochlorite to remove the organic periostracum, because the prismatic layer develops under this organic matrix. The prismatic layer records the various rates of $CaCO_3$ deposition (Fig. 10B, C), reflecting the environmental conditions during organism ontogenesis. In order to obtain the most detailed information possible from the shell microtopography, the clean shell surface is scanned using a Replica 500® 3D scanner. This scanner is of the stripe sensor type and uses the optical triangulation method to generate the range image. The spatial resolution of the scanner is 20 μm in z (altitude) and 50 μm in the x and y plane (Toubin et al. 1999). The range image dimensions (Fig. 9A) are $512 \times 128 \times 256$ (x, y, and z, i.e., the number of grey levels). Each dimension is obviously a power of 2.

The scanned prismatic shell layer is approximately 2.5 cm long and 0.7 cm wide. Because of the chosen algorithm and the image dimension ($x = 2^7$), a maximum of seven levels of resolution (or scale) is possible. For each scale, approximation and detail coefficients can be extracted. Figure 11 shows an example of the differences between image reconstruction using either approximation or detail coefficients. On the left, the approximation coefficients essentially record the general curvature of the shell, whereas the detail coefficients show an obvious cyclicity on the right hand side.

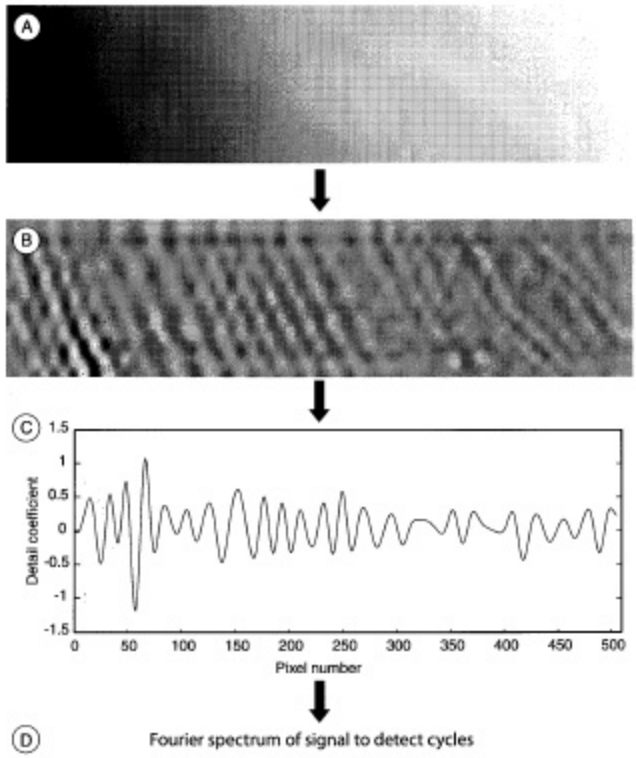

Figure 9. Method used in this paper. A) Raw range image obtained with a 3D scanner. B) Multiscalar analysis using wavelets: the raw image has been studied at seven different levels of resolution, each of them being characterized by detail and approximation coefficients. Here, the image represents the reconstruction using detail coefficients at scale 4. C) From the filtered image, a grey level line can be sampled to show the variation of detail coefficients at scale 4. D) From this 1D signal, a conventional Fourier spectral analysis can be performed in order to detect cycles.

Before performing the wavelet analysis on the raw range image, one problem is still pending. What is the significance of a growth ring? In other words, what is the relationship between pixels, prisms and time? An investigation on the prism growth rate of *A. cygnae* L. is necessary in order to determine the significance of the growth increments.

Growth increment calibration

Bivalves show differently colored bands (annuli) that are thought to be due to environmental variations such as relative content of calcium and organic matter caused by temperature or anaerobiosis (Downing et al. 1992). These factors are mainly related to climatic and seasonal variations (cold temperatures, rain and runoff waters, etc.). For example, annual winter rings can be packed as a single thick and dark annuli due to decreasing biogenic activity (cold temperature) and high dilution of calcium during rainy months. Other species simply show growth cessation during winter (after September) because the mussel becomes endobenthic, passing the winter buried in the sediment (McCuaig and Green 1982). In

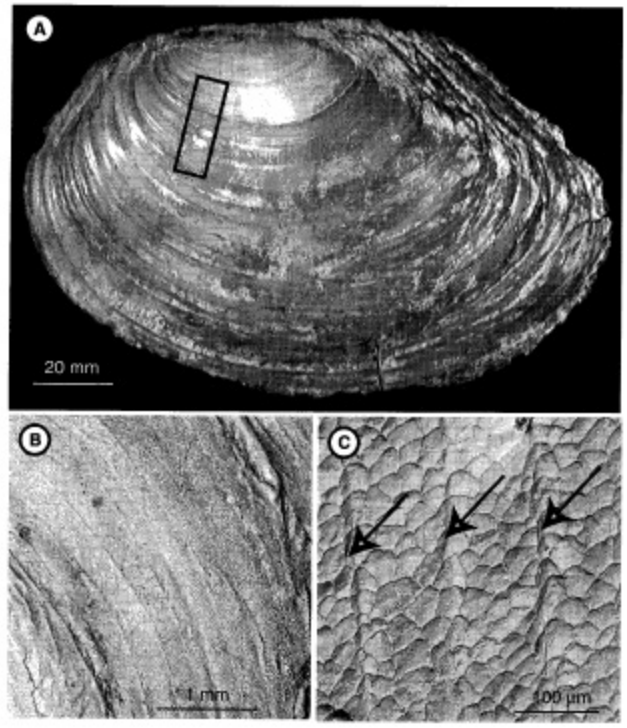

Figure 10. Example of an *Anodonta cygnae* L. specimen. A) General view of shell's external surface of the freshwater mussel. Growth rings are obvious. The black rectangle shows the approximate position of the 3D scanned surface. B) Scanning electron microscope (SEM) view of a clean surface (the organic periostracum has been removed). Multiple annuli appear, some of them being fused, showing a thicker accumulation of calcium carbonate. C) SEM view showing microtopography of the shell. The surface is constituted by the top of the prismatic layer. Three very high frequency annuli can be observed. These annuli can be detected by the resolution of the 3D scanner.

addition, some *Anodonta* form an average of 0.65 to 0.42 annulus yr^{-1}, and the rate of formation of these annuli can vary systematically with body size (McCuaig and Green 1982).

Because of the difficulty to relate growth rings to a particular time line, due to clam ontogenesis as well as their volatility to record seasonal variations, investigations have been made on the growth of *A. cygnae* L. sampled in a man-made lake at Saint-Ciergues, 70 km north of Dijon (France). The lake environment is characterized by a semi-continental climate with cold winters, mild summers, 80 to 100 days of frost and 800 to 1000 mm of precipitation per year. Sediments are mainly constituted by calcareous muds originating from the marly watershed.

The best method to evaluate the growth rate is to consider each dark ring as a mark without any particular significance in terms of time for the moment. A population of 14 individuals of the same area have been used to plot increments. Increments have been identified using the variable darkness of lines on the shell surface. In "*Anodonta*, rings are especially clear" (McCuaig and Green 1983, p. 437). The Ford-Walford plot (Walford 1946) is used to calculate an unbiased index of growth, k, because it is based on the regularity

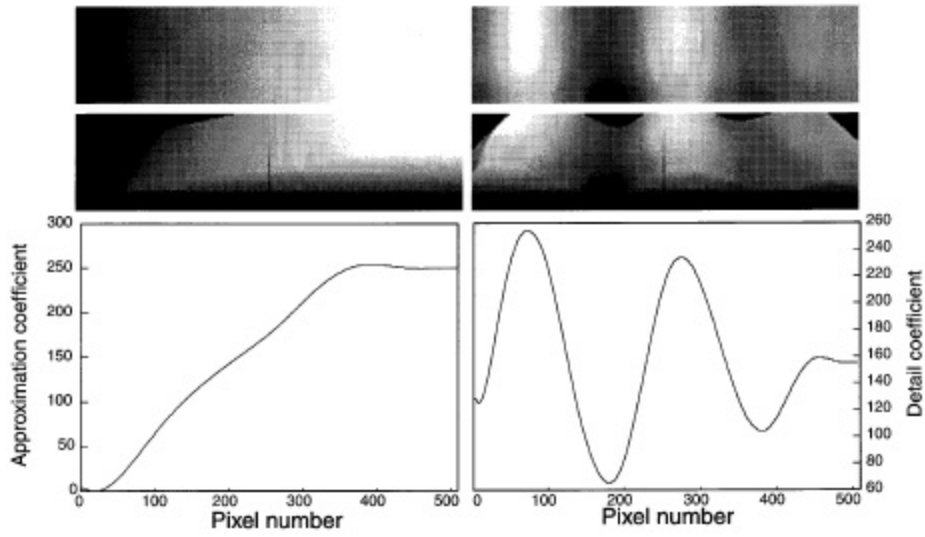

Figure 11. Example of results obtained by wavelet and multiresolution analysis on a shell range image. Left, from top to bottom: image reconstructed using approximation coefficients at scale 7. Pseudo 3D projection of the image showing the general curvature of the shell. Cross section based on approximation coefficients showing the general curvature of the shell. The plateau corresponds to a juvenile stage, when growth is fast. Right, from top to bottom: image reconstructed using only detail coefficients at scale 7. Pseudo 3D projection of the image showing that the general curvature of the shell is not visible anymore. The analysis "flattens" the shell. Cross section based on detail coefficients showing at least three main growth rings at this scale. One pixel represents two days of growth.

rather than the annularity of growth increments. The growth of a bivalve shell is generally described by von Bertalanffy's (1938) equation:

$$L_t = L_\infty\left(1 - e^{-k(t-t_0)}\right), \tag{11}$$

where L_t represents the length of the organism at time t (age), L_∞, the asymptotic length, i.e., the theoretical maximum length an organism would reach at an infinite age, k, Brody's growth constant depicts the rate at which the organism's size approaches L_∞, and t_0, the theoretical time at which we have L_0 (Anthony et al. 2001). The higher the k value, the more slowly growth approaches the limiting length (Walford 1946). The equation's parameters can be estimated using linear regression analysis of the Ford-Walford plot (Anthony et al. 2001). Therefore,

$$L_\infty = \frac{a}{1-b} \tag{12}$$

and

$$k = -\ln b. \tag{13}$$

As Anthony et al. (2001) noted, in the absence of a known age-at-length relationship, t_0 of equation (11) is impossible to estimate. Anthony et al. (2001) propose a reinterpretation of

von Bertalanffy's equation by introducing the parameter L_0 instead of t_0 as suggested by Southward and Chapman (1965), leading to the following equation:

$$L_t = L_\infty - (L_\infty - L_0)e^{-kt} \tag{14}$$

L_0 is still difficult to estimate, but Anthony et al. (2001) propose to take the glochidia (mussel larvae) as a plausible approximation of size at $t = 0$. This size is around 0.35 mm in the case of *A. cygnae* L. (Bauer 2001). Equation (14) can be rearranged in terms of time as a function of length, as proposed by Anthony et al. (2001):

$$t = \ln\left[-\frac{(L_t - L_\infty)}{(L_0 + L_\infty)}\right] \times \left[-\frac{1}{k}\right]. \tag{15}$$

The Ford-Walford plot provides the values for $a = 8.577$ and $b = 0.937$ used in equations (12) and (13). In the *Anodonta* samples from Saint-Ciergues, $k = 0.065$ ($\log k = -1.18$) and $L_\infty = 135.935$ mm. The value of k for this kind of freshwater mussel is low but consistent with the ones given by Bauer (2001, p. 236, e.g., $\log k = -1.02$) or calculated by Anthony et al. (2001, p. 1352, e.g., $k = 0.055$ for the freshwater Unionidae *Lampsilis siliquoidea*). In addition, the ecological environment of the Saint-Ciergues lake probably provides not more than 260 days of active biomineralization for *A. cygnae* L., due to long winter cold conditions.

Using all this information, it is possible to approximate the mean growth rate of *A. cygnae* L. at Saint-Ciergues. The part of the shell that has been 3D scanned belongs to the juvenile and medium period of growth. The total distance from the umbo to the end of the range image is 33 mm (Fig. 10A). The general curvature of the scanned part is shown in Figure 11 by the approximation coefficients. There is a plateau, corresponding to the end of the fast juvenile growth, followed by a slope attributed to a slower development of the shell. Nevertheless, a mean growth rate can be calculated, providing an approximation for the general growth constant. Using equation (15), the age of the shell from the umbo to the end of the part scanned can be calculated with $L_0 = 0.35$ mm, $L_\infty = 135.93$ mm, $k = 0.065$, and $L_t = 33$ mm. The result gives an age of 4.31 years. This figure is perfectly reasonable: on Figure 11, the detail coefficients shows three main increments and, on Figure 10A, it can be seen that at least one more major annulus can be added to the 3D scanned zone. It seems likely that, in this case, the major increments could be related to annual rings. Another age has been calculated on the largest and oldest *A. cygnae* L. sampled at Saint-Ciergues using the same variables but with $L_t = L_{\max} = 95.5$ mm. The result gives an age of 18.69 years. This figure is still reasonable regarding the oldest possible age for *A. cygnae* L. Using these ages, it is possible to calculate an approximation of the growth rate in μm per day.

Considering that biomineralization is effective 260 days a year, the shell part between the umbo and the end of the scanned zone has a mean growth rate of:

$$\frac{33,000}{4.31 \times 260} = 29.4\,\mu\text{m} \cdot \text{d}^{-1}. \tag{16}$$

This figure has to be considered as a sort of an average between the juvenile fast growth step and its slower development in the older part. If the total shell is included in the calculation, a figure of 19.37 $\mu\text{m} \cdot \text{d}^{-1}$ is obtained. For the part of the shell studied (the 2.5 cm scanned), a mean of 25 $\mu\text{m} \cdot \text{d}^{-1}$ seems perfectly reasonable. This rate is also confirmed for this shell

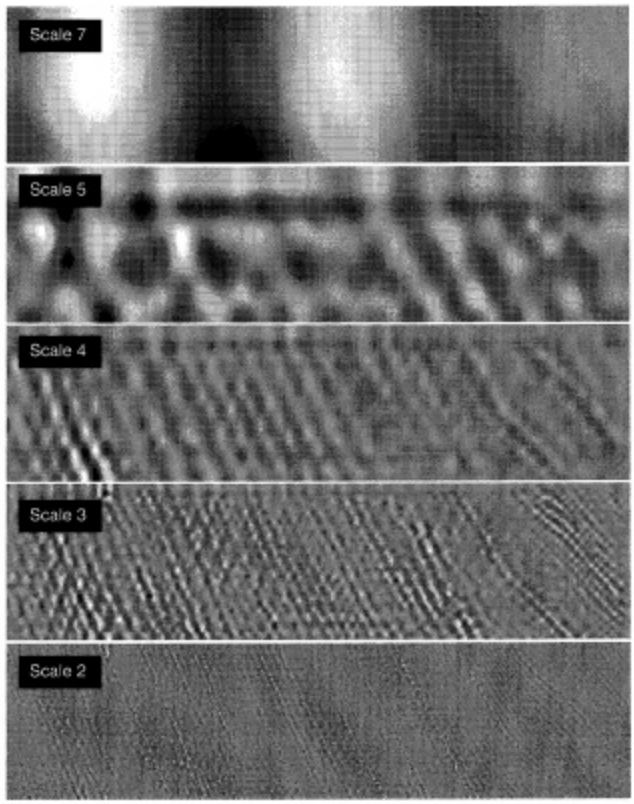

Figure 12. Reconstructed images at different scales (7, 5, 4, 3 and 1) showing the various frequencies of growth increments. Images have been built using detail coefficients for each scale.

size by extrapolation of Ravera and Sprocati (1997)'s growth curve for *A. cygnae* L. from northern Italy. To our knowledge, there is no other information available in the literature. Consequently, a range image pixel has to be considered as an integration of two days of growth on average (the xy plane resolution of 50 μm divided by the biomineralization rate 25 $\mu\text{m} \cdot \text{d}^{-1}$).

Results of spectral analysis

Today, spectral analysis is a routine method to extract cyclicity from signals. It has been used with various success on marine shells, demonstrating the existence of semi-annual, monthly (with modulations) or fortnight periodicity (e.g., Rosenberg and Runcorn (1975)). The multiresolution analysis facilitates "noise" removal by focusing on each scale of the shell record. It also drastically diminishes the interactions of frequencies due to missing or superimposed increments or random phase changes during shell growth, which obviously result in spurious peaks in the power spectrum. Nevertheless, as in conventional spectral analysis on natural objects, each milestone of natural cycles is characterized by a family of frequencies rather than a single and isolated peak (Fig. 12).

The frequency f is calculated as follows, n being an integer increment from 1 to 256:

$$f = \frac{n}{512}. \tag{17}$$

Therefore, the period is given by:

$$P = \frac{1}{f} \times 2. \tag{18}$$

Multiplying the expression by 2 allows the conversion of a period measured in pixels into a period expressed in days. The spectral analysis of the images at the various scales gives the following results:

- At scale 7: two main frequencies appear at 5.86×10^{-3} (or 341 days) and 7.81×10^{-3} (or 256 days). The first one can be considered as the annual signal, whereas the 256 day period is obviously an artifact of the dyadic algorithm ($256 = 2^8$).
- At scale 6: the same artifact at 256 days is still present, with a sub-harmonic of the 341 day period at 170 days ($f = 11.72$), confirming the semi-annual peak.
- At scale 5: two major peaks are detected, but they are difficult to interpret. They correspond to periods of 113 days ($f = 17.57 \times 10^{-3}$) and 102 days ($f = 19.53 \times 10^{-3}$).
- At scales 4, 3 and 1: the monthly modulation starts to appear at scale 4 at $f = 56.64 \times 10^{-3}$ (35 days), at scale 3 at $f = 82.03 \times 10^{-3}$ (25 days), and confirmed at scale 1 at $f = 66.84 \times 10^{-3}$ (30 days) and $f = 82.03 \times 10^{-3}$ (25 days). These monthly modulations have also been observed in marine bivalves (Dolman 1975). It is surprising to find harmonics around the 28 day lunar month in terrestrial environments. This points out a possible influence of lunar tides in lakes.
- At scales 3 and 2: the fortnight cycle (Dolman 1975) is strongly represented by a family of three peaks, at $f = 115.23 \times 10^{-3}$ (17 days) at scale 3, and at $f = 132.81 \times 10^{-3}$ (15 days) and $f = 148.43 \times 10^{-3}$ (13 days) at scale 2.
- At scale 1: in addition to the monthly cycle described above, three other peaks confirm periods already observed: the 341 day one and the artifact period at 256 days, accompanied by its 128 days (2^7) sub-harmonic.

Conclusion

The multiresolution analysis using B-splines seems to be well adapted to extract spatial as well as frequency information from natural objects. Reconstruction of an image with given approximation or detail coefficients at chosen scales allows the filtration of a specific frequency band from the initial range image and visualization of the result, keeping spatial information. These results reveal details that are drowned out in the original raw signal. However, there is still a lot of work to do to develop new wavelet filters with better accuracy. In addition, multiresolution analysis based on the dyadic method remains a limited approach

for scale resolution (which has to be a power of 2). Detection of natural cycles in natural objects using wavelet transform and multiresolution analysis is not only a challenge but also a promising field for research in paleontology as well as in sedimentology.

The researcher interested in the use of wavelet transform, but not in computer programming, can find an extremely useful and free wavelet toolbox, called "Wavelab", composed of Matlab® routines and functions. Wavelab can be found at this website: http://www-stat.stanford.edu/ wavelab/. Mathworks Inc., who distribute Matlab® software, also developed a powerful and user friendly "Wavelet toolbox". But this toolbox is not free. A lot of software information and absolutely brilliant explanations of the use of wavelet transform can be found in Addison (2002).

Summary

Conventional spectral analysis is mainly based on Fourier transform. This kind of transform provides excellent information in terms of frequencies (with their associated amplitudes) constituting the original signal, but does not keep the spatial information: it is possible to determine the elementary bricks that compose the signal, but not the way they are ordered along the signal. This limitation of the method has been noticed by Gabor (1946) who proposed a sliding window along the signal, in which the Fourier transform could be performed. In this way, part of the local (spatial) information is not lost. Nevertheless, this time-frequency tiling is still rigid and not really appropriate for natural complex signals. In the eighties, mathematicians introduced the concept of wavelet transform. The wavelet is a localized function, sort of a probe, capable of dilation (spreading out of the wavelet along the Oy axis) and translation (along the Ox axis). The transformation of the original signal by the wavelet results in coefficients, which are another expression of the signal. In addition, the wavelet transform acts as a mathematical microscope. In the discrete wavelet transform, two wavelets are used: the mother wavelet (the probe) and the scaling function. Therefore, it is possible to observe the signal at various scales, which is equivalent to the extent of the smoothing effect on the signal. This results in approximation coefficients computed by the scaling function. However, the mother wavelet will provide the detail coefficients. In conclusion, the signal is decomposed in two series of coefficients for each scale of observation. This extremely powerful tool has been used to detect cycles in the growth of lacustrine shells. By removing detail and/or approximation coefficients at different scales, and using image reconstruction (the wavelet transform has an inverse wavelet transform), annual, seasonal, tidal (monthly), and fortnight cycles in shell growth increments can easily be detected. Because of the very low amplitude of some of these cycles, it would not be possible to detect them without using the scaling effect and the detail coefficients associated with the lower scales. This method is much more powerful than the conventional Fourier transform when the aim of the study is to look for specific local periods and scale-sensitive information.

Acknowledgments

The author is indebted to many colleagues and doctoral students who helped him with the tough concept of wavelet transform. Professors F. Truchetet and A. Diou (Le2i, CNRS,

University of Burgundy, France) have been the main contributors, as well as Drs C. Dumont and M. Toubin. Dr A. Quinquis substantially improved the first draft of this manuscript. Dr P. Francus is particularly acknowledged for his patience and kindness during the chapter editing. This work has been partly funded by the Swiss National Foundation.

References

Addison P.S. 2002. The Illustrated Wavelet Transform Handbook. Institute of Physics Publishing, Bristol, 353 pp.

Anthony J.L., Kesler D.H., Downing W.L. and Downing J.A. 2001. Length-specific growth rates in freshwater mussels (Bivalvia: Unionidae): Extreme longevity or generalized growth cessation? Freshwater Biol. 46: 1349–1359.

Bauer G. 2001. Framework and driving forces for the evolution of Naiads life histories. In: Bauer G. and Wächtler K. (eds), Ecology and Evolution of the Freshwater Mussels Unionoida, Springer Verlag, Berlin, Ecol. Studies 145, pp. 234–255.

Burke Hubbard B. 1995. Ondes et ondelettes, la saga d'un outil mathématique. Pour la Science, Belin, Paris, 236 pp.

Daubechies I. 1988. Orthonormal bases of compactly supported wavelets. Comm. Pure Appl. Math. 41: 919–996.

Delyon B. 1993. Ondelettes orthogonales et bi-orthogonales. IRISA, Rennes, Publ. Int. 732, 24 pp.

Diou A., Dumont C., Laligant O., Toubin M., Truchetet F., Verrecchia E.P. and Abidi M.A. 1999. Multiscale analysis of range image: Its use for growth increment characterization. Opt. Eng. 38: 2016–2021.

Dolman J. 1975. A technique for the extraction of environmental and geophysical information from growth records in invertebrates and stromatolites. In: Rosenberg G.D. and Runcorn S.K. (eds), Growth Rhythms and the History of the Earth's Rotation, John Wiley and Sons, London, pp. 191–221.

Downing W.L., Shostell J. and Downing J.A. 1992. Non-annual external annuli in the freshwater *Anodonta grandis grandis* and *Lampsilis radiata siliquoidea*. Freshwater Biol. 28: 309–317.

Gabor D. 1946. Theory of communication. J.I.E.E. London 93: 429–457.

Mallat S. 1989a. Multiresolution approximations and wavelet orthonormal bases of L2(R). Trans. Am. Math. Soc. 315: 69–87.

Mallat S. 1989b. Multifrequency channel decomposition of images and wavelet models. IEEE Trans. Acoustic Speech and Signal Proc. 37: 2091–2110.

Mallat S. 1989c. A theory for multiresolution signal decomposition: The wavelet representation. IEEE Trans. Pattern Anal. Mach. Intell. 11: 674–693.

McCuaig J. and Green R.H. 1982. Unioid growth curves derived from annual rings: A baseline model for Long Point Bay, Lake Erie. Can. J. Fish. Aquat. Sci. 40: 436–442.

Meyer Y. 1990. Ondelettes et Opérateurs I. Hermann, Paris, 215 pp.

Olkkonen H. 1995. Discrete binomial splines. Graph. Models and Image Proc. 57: 101–106.

Ravera O. and Sprocati A.R. 1997. Population dynamics, production, assimilation and respiration of two fresh water mussels: *Unio mancus* Zhadin and *Anodonta cygnae* Lam. Mem. Ist. Ital. Idrobiol. 56: 113–130.

Rosenberg G.D. and Runcorn S.K. (eds) 1975. Growth Rhythms and the History of the Earth's Rotation. John Wiley and Sons, London, 559 pp.

Southward G. and Chapman D. 1965. Utilization of Pacific halibut stocks: Study of Bertalanffy's growth equation. Rep. Int. Pac. Halibut Comm. 39, 33 pp.

Rhoads D.C. and Pannella G. 1970. The use of molluscan shell growth patterns in ecology and paleoecology. Lethaia 3: 143–161.

Schwarzacher W. 1993. Cyclostratigraphy and the Milankovitch Theory. Elsevier, Amsterdam, Dev. in Sedim. 52, 225 pp.

Toubin M., Dumont C., Verrecchia E.P., Laligant O., Diou A., Truchetet F. and Abidi M.A. 1999. Multi-scale analysis of shell growth increments using wavelet transform. Comp.. Geosci. 25: 877–885.

Truchetet F. 1998. Ondelettes pour le Signal Numérique. Hermès Sci. Publ., Paris, 156 pp.

Viscito E. and Allebach J.P. 1991. The analysis and design of multidimensional FIR perfect reconstruction filter banks for arbitrary sampling lattices. IEEE Trans. Circ. Syst. 38: 29–41.

von Bertalanffy L. 1938. A quantitative theory of organic growth (Inquiries on growth laws. II). Human Biol. 10: 181–243.

Walford L.A. 1946. A new graphic method of describing the growth of animals. Biol. Bull. 90: 141–147.